Photon avalanche and the mean-field approximation

S. Guy, M. F. Joubert, and B. Jacquier
Université Claude Bernard Lyon 1, UMR 5620, Bât 205, 69622 Villeurbanne Cedex, France
(Received 12 November 1996)

Starting from a microscopic description, we show the analogy between photon avalanche and second-order phase transition. This justifies the validity of the mean-field approximation. Then we show that the rate equations reproduce quantitatively the experimental results as soon as the Gaussian intensity profile of the input beam is taken into account. Moreover, we apply the general Landau theory to the photon avalanche: the absorption between the excited state is the control parameter of the transition whereas the ground-state absorption is an external field. By this way the impact of the residual nonresonant ground-state absorption is clarified. [S0163-1829(97)03913-1]

I. INTRODUCTION

Demonstrations of upconversion pumped solid-state lasers have enhanced the interest in excitation mechanisms that result in emission at wavelengths shorter than that of the pump light. Efficient upconversion is possible in rare-earth (RE)-doped materials with metastable, intermediate levels that can act as a storage reservoir for the pump energy. Subsequent emission from higher lying states can be induced by excited state absorption (ESA) of pump photons, or by energy transfer processes. The photon avalanche is an unconventional continuous waves pumping mechanism because it leads to strong upconverted emission without any resonant ground-state absorption (GSA). The pump wavelength is only resonant between the metastable state and a higher energy level. The main characteristic of such a process is a pump power threshold which clearly separates two different regimes: below, the upconverted fluorescence intensity is weak and the crystal is transparent to the pump; above, the fluorescence increases by orders of magnitude and the pump light is strongly absorbed. In the same way, there is a change of the rise shape of the transient signals as well as a very important slowing down at the threshold.

Since its discovery in Pr^{3+}-doped materials,[1] the photon avalanche effect has been demonstrated in many other rare-earth or Ni^{2+}-doped materials.[1–22] Moreover, a recent study of Tm^{3+}-doped CdF_2 demonstrated that, in this system, the photon avalanche is the most efficient upconversion process leading to population inversion.[23] Blue laser emission under avalanche pumping schemes was achieved in $LiYF_4:Nd^{3+}$ (Ref. 2) and $LiYF_4:Tm^{3+}$ (Ref. 3). More recently,[13] avalanche pumped upconversion $YAlO_3:Er^{3+}$ green laser was reported, although in this case, dynamics that explicitly verifies the pumping mechanism was not presented. Unfortunately, all these devices work only at cryogenic temperature. However, among bulk systems, they belong to the most efficient upconversion lasers. In order to optimize avalanche-pumped lasers, aiming, e.g., room-temperature operation, a good knowledge of the avalanche mechanism is a prerequisite.

Some papers tried to give a general and theoretical approach to the photon avalanche. The microscopic mechanism, responsible for the self storage of the metastable level, was immediately identified.[1] The macroscopic point of view was treated with the help of the general rate equation analysis and it has been shown that such a mean-field approach gives good qualitative description of most of the experimental results.

(i) A pump intensity threshold corresponding to a bifurcation of the rate equation stationary solutions.[8,23,24]

(ii) This threshold exists only for high enough active ion concentration.[8,23,24]

(iii) A slowing down and a change of the excited state population rise shape at threshold.[2,8,23]

But, unfortunately, different attempts to fit the data (fluorescence intensity versus pumping rate and transient signals) above the threshold were unsuccessful with rate equation.[10,15] Moreover, some authors pointed out recently that this mean-field approach failed to give the qualitative feature of the key metastable level[9] (this theory predicts a rapid buildup of the population of that level versus pumping rate and a subsequent depletion, while the experimental results show a slow buildup).

Our interest is twofold: to show that we do not lose anything of the microscopic model by doing the average field approximation and also to identify the reason for which previous fitting above the threshold did not work.[10,15,9] In doing so, we confirm that the photon avalanche is a bifurcation phenomenon. In the first part of this paper, starting from a microscopic description, we show that photon avalanche is analogous to second-order phase transition. Then, we explain why the mean-field approach remains correct to describe this process. We use the well known Landau theory to emphasize the physics contained in the rate equations. This powerful formalism is very well adapted to study the impact of the residual ground-state absorption. By this way, we define the absorption cross section conditions for which the photon avalanche remains the main pumping channel for the upconverted fluorescence. In the last part, we identify an experimental parameter, the pump beam profile, which reconciliates rate equations with experimental data.

As the photon avalanche experimental results presented in this paper are related to the strong blue (485 nm) emission of Tm^{3+} ions in a 5 at. % doped yttrium aluminum garnet (YAG) single crystal after red cw pumping, we focus also on this trivalent RE ion for the theoretical treatment. But, what-

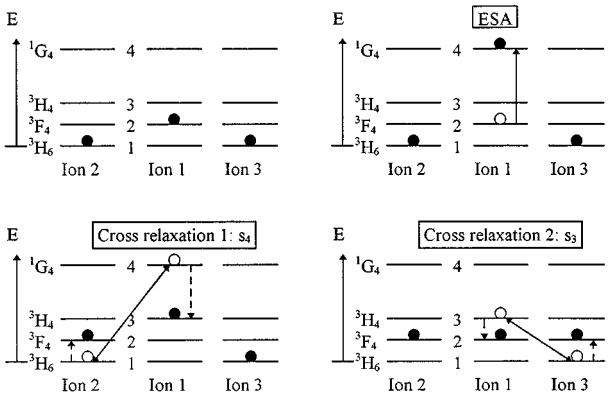

FIG. 1. Microscopic description of the photon avalanche pumped $^1G_4 \rightarrow {}^3H_6$ emission of Tm^{3+}.

ever is the photon avalanche system, the results are analogous.

II. MICROSCOPIC DESCRIPTION AND MEAN-FIELD APPROACH

To keep the clarity of this paper, we remember the microscopic description of the photon avalanche process leading to the strong blue emission ($^1G_4 \rightarrow {}^3H_6$) of Tm^{3+} after red excitation resonant with the $^3F_4 \rightarrow {}^1G_4$ transition.[3] It is schematized in Fig. 1. As all ions are initially in the ground state 1 (no thermal population of level 2), the effect of the pump is minimal. If one ion is promoted to the metastable state 2, whatever is the mechanism of population of this state, it may be further excited to level 4 by absorption of the pump photon. Then, due to high concentration this ion can interact with two neighbors: a first cross relaxation energy transfer (CR) promotes one neighbor ion into the $^3F_4$ level, the initial excited ion decaying to the $^3H_4$ state 3 from which another CR results in two other ions in the metastable level. Now, three ions are available for further absorption of the pump light. After, by the same feeding process, nine ions are excited to the metastable state and so on. This description is phenomenologically identical to that given for the most simple photon avalanche case where only one CR is involved[1,2] leading to only two ions in the metastable state and so on.

Just by having a look on that microscopic process we see an evident analogy with second-order phase transition of ferromagnetic spin systems. For the avalanche, each ion excited in the metastable state interacts, due to the pump beam and the CR, with its neighbors in such a way that they all lie in this state. The avalanche (without GSA) excited population is the result of the competition between the self storage, which puts all the ions in the metastable state, and the losses of the level 2, which have the opposite effect.[25] The pumping rate between excited states controls the interactions between ions by allowing or not the CR. For the avalanche as well as for spin systems, the interactions between ions connect them with each other in order to put all of the ions in the same state (metastable state or spin aligned state respectively). While the pumping rate between excited state controls these interactions for the avalanche, the temperature is the controlling parameter in the case of the ferromagnetism. Moreover, as an external magnetic field for spin systems, the residual absorption from the ground state can be seen as an external field which puts all the ions in the metastable state whatever the control parameter (excited state pumping rate) may be. This analogy of the photon avalanche as such a nonlinear process is very important because many studies were done on this general field and especially on the validity of the average field approximation. Normand[26] demonstrated, as a general rule, that the mean-field approach (rate equations) for second order phase transition and more generally for bifurcation, is valid except in the extreme vicinity (10^{-4}–10^{-5}) of the bifurcation point, for which the fluctuations take a great importance.

As soon as we do not approach so tightly the critical point, we may give a simple and clear interpretation of this process by using the following rate equation description of the microscopic process depicted in Fig. 1:

$$dn_4/dt = R_2 n_2 - W_4 n_4 - s_4 n_1 n_4, \tag{1}$$

$$dn_3/dt = R_1 n_1 - (W_3 + W_3^{\mathrm{NR}}) n_3 + b_{43} W_4 n_4 + s_4 n_1 n_4 - s_3 n_3 n_1 + Q_{23} n_2^2, \tag{2}$$

$$dn_2/dt = -(R_2 + W_2) n_2 + b_{42} W_4 n_4 + (b_{32} W_3 + W_3^{\mathrm{NR}}) n_3 + s_4 n_1 n_4 + 2 s_3 n_1 n_3 - (Q_{22} + 2Q_{23}) n_2^2, \tag{3}$$

$$n_1 + n_2 + n_3 + n_4 = 1. \tag{4}$$

Except the Q_{ij} terms, which will be explicited later in this section, this system was used previously.[10,15] It is assumed that the first step promoting at least one ion in $^3F_4$ occurs via the nonresonant phonon sideband GSA above the $^3F_2$ level followed by fast nonradiative decay to $^3H_4$. Then, different deexcitation channels can feed up the metastable level. So, equations (1)–(4) involve the ground- and excited-state pumping rates R_1 and R_2, the single ion radiative relaxation rates W_i of level i and the branching ratios b_{ij} from level i to level j. The multiphonon relaxation rate from level 3, W_3^{NR}, is the only one which cannot be neglected. The CR energy transfers are described by the parameters s_3 and s_4 which induce nonlinear terms in the rate equations. At high excitation power, the metastable state population is high enough for the following saturation processes to occur.[27,28]

The inverse process of the s_3 CR:

$$^3F_4 + {}^3F_4 \rightarrow {}^3H_6 + {}^3H_4.$$

The upconversion process:

$$^3F_4 + {}^3F_4 \rightarrow {}^3H_6 + {}^3H_5,$$

followed by rapid nonradiative decay from $^3H_5$ to $^3F_4$.

These two processes are taken into account in Eqs. (1)–(4) by the terms $Q_{23} n_2^2$ and $Q_{22} n_2^2$ respectively.

III. THE LANDAU THEORY

Now, we will deduce a potential from the rate equations in order to give a clearer description of the photon avalanche. As in the Landau theory,[29] we will show that the deformation of that potential versus the pumping rate clearly separates

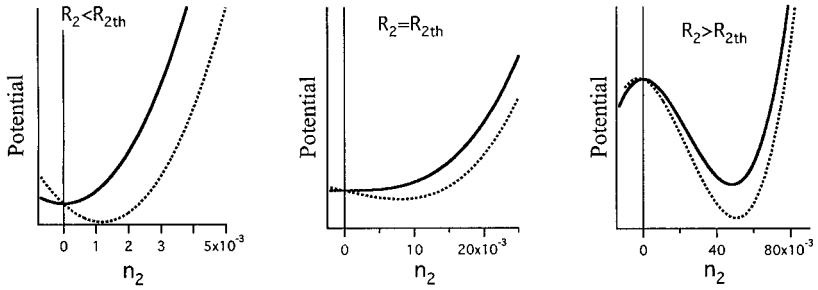

FIG. 2. Potential curves calculated for three values of the control parameter R_2, with the parameters given in Table I and in the two cases: $R_1=0$ (—) and $R_1=10^{-3}R_2$ (···).

two different pumping regimes (two different phases in the Landau theory).

Assuming quasiequilibrium of higher excited levels with the metastable one (such an adiabatic approximation being correct below and around the threshold), Eqs. (1)–(3) become

$$\frac{dn_2}{dt}=-W_2\left(1-\frac{R_2}{R_{2\mathrm{th}}(n_1)}\right)n_2+\tau_3(n_1)W_{32}(n_1)R_1n_1 -Q(n_1)n_2^2, \tag{5}$$

$$n_3(t)=\tau_3(n_1)R_1n_1+\tau_3(n_1)W_{43}(n_1)n_4+\tau_3(n_1)Q_{23}n_2^2, \tag{6}$$

$$n_4(t)=\tau_4(n_1)R_2n_2, \tag{7}$$

where

$$\tau_4(n_1)=(W_4+s_4n_1)^{-1},\quad \tau_3(n_1)=(W_3+W_3^{\mathrm{NR}}+s_3n_1)^{-1},$$

$$W_{32}(n_1)=b_{32}W_3+W_3^{\mathrm{NR}}+2s_3n_1,$$

$$W_{43}(n_1)=b_{43}W_4+s_4n_1,$$

$$Q(n_1)=Q_{22}+Q_{23}[2-\tau_3(n_1)W_{32}(n_1)],$$

$$R_{2\mathrm{th}}(n_1)=W_2/[\tau_4(n_1)W_{43}\tau_3(n_1)W_{32}(n_1) +\tau_4(n_1)W_{42}(n_1)-1].$$

Then, as below and around the threshold we may replace n_1 by $1-n_2$, Eq. (5) has the form

$$dn_2/dt=\varphi_{R_2}(n_2). \tag{8}$$

The time evolution of n_2 is induced by the force $\varphi_{R_2}(n_2)$ which is controlled by the pumping rate R_2. n_2 is the order parameter which satisfies the bifurcation equation. We define the potential $U(n_2)$ from the force φ_{R_2} as $\varphi_{R_2}(n_2)=-dU/dn_2$. The steady state solutions of n_2 are the extrema of U ($\varphi_{R_2}=0$), stable for a minimum and unstable for a maximum. We may expand φ_{R_2} and U in a power series in the order parameter n_2 in order to investigate the deformation of U under the variation of the control parameter R_2.

As typical values of the GSA pumping rate R_1 lie between 2 and 5 orders of magnitude lower than the ESA pumping rate R_2, we shall first neglect the R_1 depending terms in the expansion. Then we shall study the impact of these terms.

A. Negligible external field (GSA=0)

By assuming negligible GSA, the expressions for the force $\varphi_{R_2}(n_2)$ and for the potential $U(n_2)$ are

$$\varphi=-W_2[1-R_2/R_{2\mathrm{th}}]n_2-\{cR_2+Q\}n_2^2+\cdots, \tag{9}$$

$$U=W_2[1-R_2/R_{2\mathrm{th}}]n_2^2/2+\{cR_2+Q\}n_2^3/3+\cdots, \tag{10}$$

with

$$R_{2\mathrm{th}}=W_2[\tau_4W_{42}+\tau_4W_{43}\tau_3W_{32}-1]^{-1}, \tag{11}$$

$$c=(2-\tau_3W_{32})\tau_3s_3\tau_4W_{43}+(1-b_{43})W_4\tau_4\tau_4s_4\tau_3W_{32} +(1-b_{42})W_4\tau_4\tau_4s_4$$

in which

$$W_{4j}=b_{4j}W_4+s_4,\quad W_{3j}=b_{3j}W_3+W_3^{\mathrm{NR}}+s_3,$$

$$\tau_4=(W_4+s_4)^{-1},\quad \tau_3=(W_3+W_3^{\mathrm{NR}}+s_3)^{-1}.$$

If $R_{2\mathrm{th}}<0(\tau_4W_{42}+\tau_4W_{43}\tau_3W_{32}<1)$, the time derivative of n_2 [Eq. (8) with (9)] does not contain any positive term, so the population of level 2 could never grow and there is no avalanche. This inequality gives the condition on cross relaxation for the avalanche to occur. If $R_{2\mathrm{th}}>0$, assuming that all ions are initially in the ground state, then $R_{2\mathrm{th}}$ is the value from which the self storage of level 2 becomes more efficient than the losses.[25] In the latter case, bearing in mind the U expression, the potential curves are drawn in continuous lines on Fig. 2 for different values of R_2 relative to $R_{2\mathrm{th}}$. When $R_2<R_{2\mathrm{th}}$, only one stable solution is accessible. This is the trivial solution: no GSA leads to no excited state population ($n_2=0$). Beyond the critical value $R_{2\mathrm{th}}$ the shape of the potential changes fundamentally. A new solution appears and the trivial solution becomes unstable: the effect of fluctuations or of a small external perturbation is no longer damped. The system acts as an amplifier; it moves away from the trivial solution and evolves to a new regime: the avalanche solution (nonzero excited state population without GSA). This transformation of the potential leads to the very

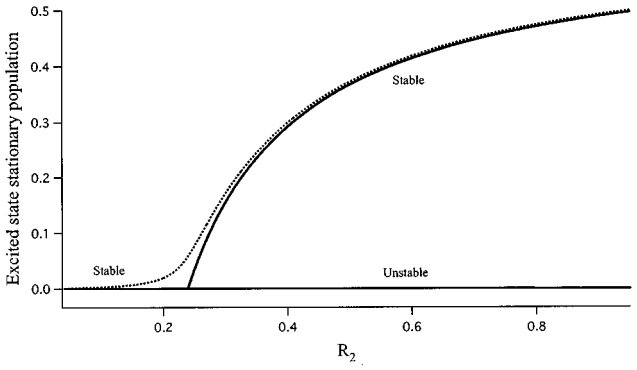

FIG. 3. Evolution of the excited state stationary population with the control parameter R_2. The curves are calculated with the parameters given in Table I and in the two cases: $R_1=0$ (—) and $R_1=10^{-3}R_2$ ($\cdots$).

simple bifurcation diagram of the stationary solution drawn in Fig. 3—the unique zero solution loses its stability at $R_{2\text{th}}$: at this value of the control parameter a new branch of solution, which is stable, is generated. Concerning the stability, we find the same result as in Ref. 8 where we studied the linear stability of the solutions of the rate equations system.

B. Impact of the external field

GSA acts on avalanche as a very small external perturbation and, in the expanded expression of φ and U this perturbation leads to the following result:

$$\varphi = aR_1 - \{W_2[1-R_2/R_{2\text{th}}]+bR_1\}n_2 - \{cR_2+Q\}n_2^2+\cdots, \tag{12}$$

$$U = -aR_1n_2+\{W_2[1-R_2/R_{2\text{th}}]+bR_1\}n_2^2/2 + \{cR_2+Q\}n_2^3/3+\cdots \tag{13}$$

with

$$a=\tau_3 W_{32},$$

$$b=(2-\tau_3 W_{32})\tau_3 s_3+\tau_3 W_{32}.$$

The impact of the GSA on the potential is given by the terms aR_1n_2 and $bR_1n_2^2/2$. The first one describes the direct feeding of the metastable state due to the GSA. As we will see later in this section, it changes deeply the shape of the potential curves. The second term does not change the physical behavior of the avalanche as a bifurcation. It can be seen as an additional loss for the metastable level. Indeed, we may rewrite Eq. (12) as

$$\varphi = aR_1 - W_2[1-I/I_{\text{th}}]n_2 - \{cR_2+Q\}n_2^2+\cdots \tag{14}$$

with

$$I_{\text{th}} = R_{2\text{th}}/\sigma_2 \times 1/(1-b\sigma_1 R_{2\text{th}}/\sigma_2 W_2), \tag{15}$$

where I is the excitation intensity in photon cm^{-2} units, σ_1 and σ_2 are the GSA and ESA cross section respectively defined by $R_i=\sigma_i I$. Now, if we forget the aR_1 term, we may see that Eq. (14) is equivalent to Eq. (9) with a new intensity threshold. So the change of the potential versus the control parameter $R_2=\sigma_2 I$ remains the same as in Sec. III A. Instead of having the excitation intensity threshold $R_{2\text{th}}/\sigma_2$, we have the little bigger value given by equation (15). That increasing is not significant as soon as R_1 is more than one order of magnitude lower than R_2.

The term aR_1 is identified with an external field in the Landau theory of phase transitions. It induces a unique solution for the system whatever the R_2 value may be, and so, diminishes the difference between the two pumping regimes (see Fig. 3). The changes in the potential well are presented in Fig. 2 in dotted lines. The dynamics of the system is directly linked to the shape of the potential. At $t=0$, the system is in the $n_2=0$ position ($R_i=0$). Then, we switch on the pumping radiation ($R_i\neq 0$), so the system now feels the macroscopic potential. It moves down the potential well more or less fast depending on the slope.

Beneath the threshold, this external field imposes the pumping regime: linear equations ($n_1\approx 1$), exponential dynamics and very weak excited state population. Above the threshold, the system is described by the avalanche potential. As soon as the GSA$\ll$ESA, the GSA pumping rate does not change dramatically the equilibrium value of the potential. But it is very important in the sense that, initially, it allows the system to fall into the well. Indeed, it only acts on the system by bending the potential at $n_2=0$ which makes the system moving into the potential well, slowly in early time then faster.

Around the threshold the potential is very flat. It means that the force $\varphi(n2)$ becomes weaker and weaker as we come nearer to the threshold. This is the critical slowing down expected for second-order phase transition.[26] Then, the time to reach the stationary solution is at a maximum. By integrating Eq. (8) with the second order of Eq. (14), we find for $I=I_{\text{th}}$

$$n_2(t)=n_2(\infty)\tanh(t/tc) \tag{16}$$

with

$$t_c = 1/\sqrt{a\sigma_1 I_{\text{th}}(c\sigma_2 I_{\text{th}}+Q)} \tag{17}$$

The dynamics presents an hyperbolic tangent profile of time constant t_c which, for a small GSA ($I_{\text{th}}\approx R_{2\text{th}}/\sigma_2$), is given by

$$t_c \approx \frac{1}{\sqrt{aR_{2\text{th}}(cR_{2\text{th}}+Q)}}\sqrt{\frac{\sigma_2}{\sigma_1}} \tag{18}$$

Moreover, for a long metastable state lifetime $\tau_2=W_2^{-1}$, $cR_{2\text{th}}\ll Q$. Inserting the expression of $R_{2\text{th}}$ [Eq. (11)] into Eq. (18) leads to

$$t_c \approx \sqrt{\frac{\tau_4 W_4+\tau_4 W_{43}\tau_3 W_{32}-1}{aQ}}\sqrt{\frac{\tau_2\sigma_2}{\sigma_1}}. \tag{19}$$

Finally, the critical slowing down at threshold t_c/τ_2 which is the signature of photon avalanche, is proportional to $\sqrt{\sigma_2/\tau_2\sigma_1}$. So the more σ_1 is low compared to σ_2, the more the slowing down should be spectacular. Examples of experimental rise curves are presented in Fig. 4 in the case of YAG:5 at. % Tm^{3+}. The different pumping regimes are clearly identified with a drastic slowing down at threshold (250 ms for a metastable state lifetime of 12 ms). The reason

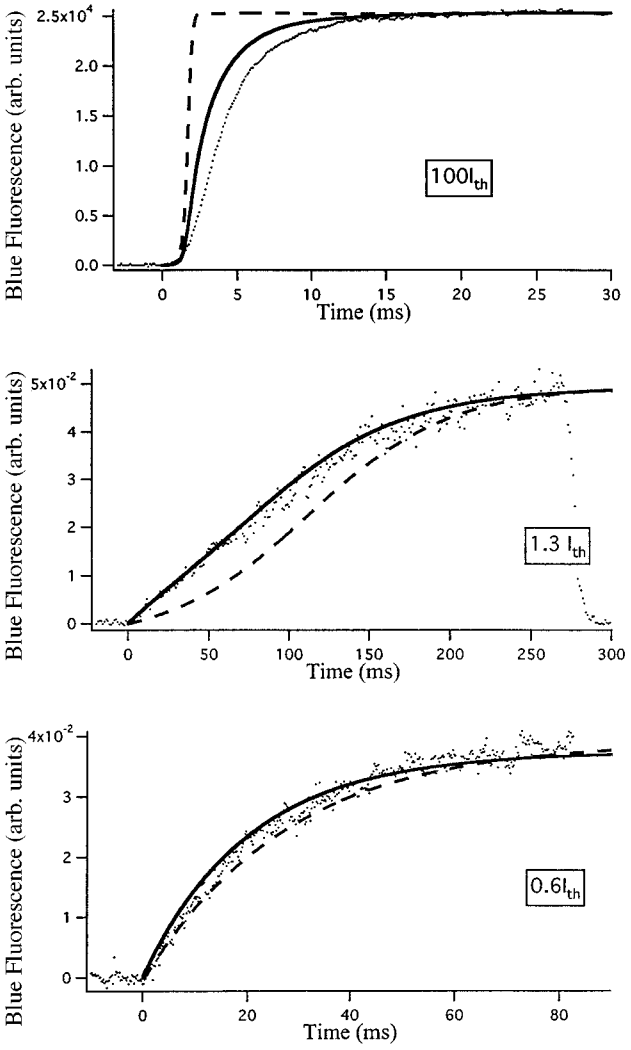

FIG. 4. Experimental rise curves ($\cdots$) of the n_4 population for different pump intensities in YAG:5 at. % Tm^{3+} at 35 K using the experimental setup described in Ref. 8. Note the time scale at the apparent experimental threshold ($I=1.3I_{th}$). Theoretical curves are calculated for top hat (- - -) or Gaussian (—) input beam profile.

for which the experimental intensity threshold is equal to $1.3I_{th}$ will be given in Sec. IV.

C. Relative contributions of GSA and avalanche pumping

In typical avalanche experiment, the GSA is much weaker than the ESA, then the impact of the GSA is only to allow the system to leave from the initial position ($n_2=0$) to the avalanche solution. However, if the GSA is more significant, it could become the principal pumping channel.[30] In the right part of equation (14) the direct population of the metastable state by the GSA is given by the term aR_1 whereas the population due to the avalanche is given by the linear and quadratic n_2 terms. This leads to an easy way to determine which kind of pumping (avalanche or GSA) is preponderant. Beneath the avalanche threshold, the GSA is obviously the main pumping route. Above the threshold, we shall use the susceptibility of the external field aR_1 to differentiate the two mechanisms. We define it in a common way as:

$$\chi=\left(\frac{\partial n_2}{\partial aR_1}\right)_{R_{2=cste},aR_1\to 0}. \tag{20}$$

By differentiating Eq. (14) in the stationary regime ($\varphi_{R_2}=0$), we extract the expression

$$\frac{\partial n_2}{\partial aR_1}=\frac{1}{W_2(1-I/I_{th})+2(cR_2+Q)n_2} \tag{21}$$

n_2 is the solution of Eq. (14) when $aR_1=0$ (e.g., the avalanche solution)

$$n_{ava}=-W_2(1-I/I_{th})/(cR_2+Q), \quad \text{when } I>I_{th} \tag{22}$$

$$n_{ava}=0, \quad \text{when } I<I_{th}.$$

We inject these expressions in Eq. (21) to find:

$$\chi=\frac{1}{W_2\left|1-\frac{I}{I_{th}}\right|}. \tag{23}$$

The GSA leads to the excited population

$$n_{GSA}=\chi aR_1. \tag{24}$$

The susceptibility diverges at the avalanche threshold (Curie law[29]) because the potential is very flat and so, even a very small perturbation acts significantly on the system. It means that near the threshold the relative population induced by the GSA is the biggest, but, when the input intensity increases the susceptibility goes down and so the avalanche pumping could become preponderant. From the expressions of n_{GSA} [Eq. (24)] and n_{ava} [Eq. (22)] we can determine the intensity value for which the avalanche pumping is the main route, i.e., $n_{ava}>10n_{GSA}$. We find easily

$$n_{ava}>10n_{GSA}\Leftrightarrow f(I)=(10ac\sigma_2^2\beta-W_2^2/I_{th}^2)I^2$$
$$+(10a\sigma_2\beta Q+3W_2^2/I_{th})I-W_2^2<0$$

with $\beta=\sigma_1/\sigma_2$. This function is a parabola with its concavity up or down depending on the sign of the quadratic coefficient.

First case: $\beta>\beta_0=W_2^2/(10ac\sigma_2^2I_{th}^2)$.

The quadratic coefficient is positive, so the concavity is up. Moreover, the derivative is positive whatever $I>I_{th}$ and $f(I_{th})=10a\sigma_2\beta I_{th}(c\sigma_2 I_{th}+Q)>0$. Then, we may conclude that, in that case, $f(I)>0$ whatever $I>I_{th}$ (see Fig. 5) and so the main pumping regime is never the avalanche pumping.

Second case: $\beta<\beta_0$.

Now, the graph of $f(I)$ is a parabola with the concavity down [$f(\infty)=-\infty$]. As $f(I_{th})$ remains positive, we may conclude that, at threshold, the metastable state is essentially populated via direct GSA. Moreover, there is only one root greater than I_{th} (see Fig. 5), $f(I)$ is positive before that root and becomes negative when I is greater. So, just above the threshold, there is always a region where the GSA is the main pumping regime. We switch to the avalanche pumping regime by improving the intensity. So theoretically, a regime of avalanche pumping could happen providing that $\beta<\beta_0$.

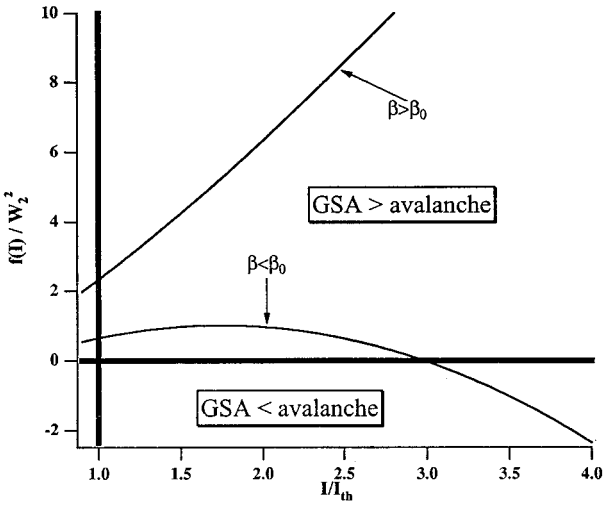

FIG. 5. Calculated evolution of the function $f(I)$ determined in the text. $f(I)$ measures the relative efficiency of the two pumping mechanisms (avalanche and GSA). When $f(I)$ is positive the GSA is the main pumping mechanism, when it is negative this is the opposite.

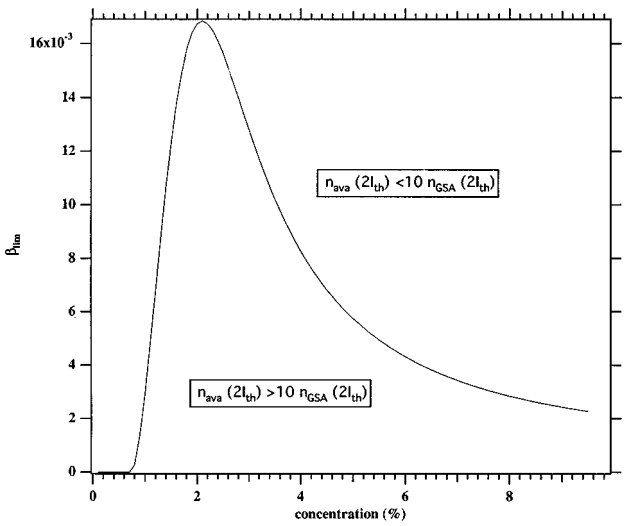

FIG. 6. Calculated evolution of the limit ratio σ_1/σ_2 for which the avalanche becomes the main pumping mechanism as soon as $I>2I_{\text{th}}$. We take the case of YAG:Tm^{3+} using the parameters given in Table I and the following concentration dependencies where c is in at %: $s_3(\text{ms}^{-1})=1.6\ c^2$ (Ref. 34), $s_4(\text{ms}^{-1})=1.16\ c^2$ (Ref. 33), $Q_{22}=0.32c^3/(c^2+4.3^2)$ and $Q_{23}=0.09c^3/(c^2+4.3^2)$ (Ref. 28).

Experimentally, the excitation intensity value for which $f(I)=0$ should not be to big to be detected. We may take $f(2I_{\text{th}})<0$ as the limit to detect the avalanche regime. It means that for $I>2I_{\text{th}}$ the population due to the avalanche pumping is at least ten times bigger than that one given by the GSA pumping. If we choose to detect the avalanche pumping for bigger value of the intensity, it will lead to a bigger limit for β. $f(2I_{\text{th}})<0$ leads to the limit on β,

$$\beta<\beta_{\text{lim}}=5\ \ 10^{-2}W_2{}^2/[aR_{2\,\text{th}}(Q+2cR_{2\,\text{th}})]. \qquad (25)$$

So β_{lim} depends on the rare earth host as the parameters of Eq. (25). Moreover, for a given host, β_{lim} depends on the rare-earth concentration as the parameters a, c, and Q. The variation of β_{lim} versus concentration is given on Fig. 6 in the case of YAG:Tm^{3+}.

In the most simple photon avalanche case (three levels) there is only one CR.[1,2] The treatment of the corresponding rate equation system leads to the same expressions for Eqs. (8)–(25). The only difference arises from the expression of the constants a, b, c, Q, and $R_{2\text{th}}$ (see Appendix). In a recent paper,[31] the authors claimed a limit value of β, in the three-level case, for the avalanche behavior nearly independent of the considered compound and much lower than our result. The difference arises from the fact that their limit does not differentiate from the two pumping mechanisms. It is only a visual limit for which the curve of the upconverted population versus the pumping rate is not too far away from the pure avalanche case ($\beta=0$). Moreover, as their numerical calculations are made at the threshold point, for which GSA is the main pumping mechanism, they can not measure the limit of the avalanche efficiency.

IV. FITTING PROCEDURE

The rate equation analysis shows that the photon avalanche is a macroscopic effect governed by the macroscopic force $\varphi(n_2)$. The validity of this mean-field approach is linked to the relatively high active ion concentration. Indeed, in material presenting the photon avalanche effect, the rare-earth doping level is usually high enough for the mean radius between active ions to be smaller than the average interaction length. So, all the ions are connected to each other and no clustering effect has to be considered. Moreover, as already mentioned in Sec. II, the mean-field approach for phase transitions, and more generally for bifurcation, is valid except in the extreme vicinity of the critical point,[26] for which susceptibility and correlation length diverge. Experimentally we are not able to investigate so precisely the threshold, so the rate equation model should fit properly experimental data.

In the case of YAG:5 at % Tm^{3+}, our experimental results obtained at 35 K are presented in Figs. 4 and 7. The transient signal of the upconverted blue fluorescence has been recorded for more than 30 different pumping powers. Three of them are drawn in Fig. 4. Figure 7 shows the fluorescence intensity from both the metastable and upconverted level versus the input power under stationary condition ($t=\infty$).

The intensity profile of the pump laser beam, which is roughly Gaussian, is an essential experimental parameter. This feature was first pointed out from a phenomenological model of the avalanche.[32] Surprisingly, nobody, even the authors of Ref. 32, applies this aspect to rate equations. In an experiment, the transversal collected fluorescence (proportional to the concerned population), as well as the transmission, result from all the parts of the pump beam. The great importance of avalanche (as with other bifurcation processes) rests in the fact that even a small change of the control parameter R_2 leads to a dramatic change of the system. Therefore, inside the beam, we could find fractions of ions with very different fluorescence dynamics and intensities according to the incident intensity value versus the threshold. The summation of all these contributions may not be equal to that given by an average input intensity. We are therefore

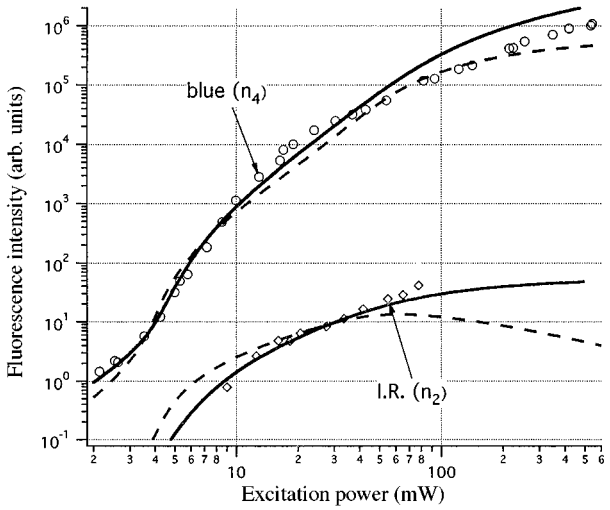

FIG. 7. Experimental variation of the blue from $^1G_4$ (○) and the IR from $^3F_4$ (□) fluorescence versus the excitation power in YAG:5 at. % Tm^{3+} at 35 K using the experimental setup described in Ref. 8. Theoretical curves are calculated for top hat (- - -) or Gaussian (—) input beam profile.

obliged to integrate over the Gaussian input intensity profile of the beam. When the intensity I_0 at the center of the pump beam is above the intensity threshold, the wings of the beam, where the intensity is less than I_0 but still above or around the threshold, give rise to slower dynamics. So a Gaussian averaging should induce a great slowing of the fluorescence rise. When the intensity I_0 at the center of the pump beam is beneath the intensity threshold, the effect is exactly the opposite. So, the input intensity for which the experimental transient has the characteristic shape of the phase transition (very slow quasilinear risetime) will be a little bit higher than I_{th}.

As the differential equations of Eqs. (1)–(4) cannot be solved explicitly, the theoretical curves presented in Figs. 4 and 7 are obtained by numerical calculation of Eqs. (1)–(4). To perform the resolution, radiative and nonradiative relaxation rates as well as cross relaxation transfer rates were measured by other spectroscopic experiments[28,33,34] and given in Table I. So, except the absorption rates R_1 and R_2, all the spectroscopic parameters are known and fixed. Then, each experimental transient curve is fitted by resolving the system I for pumping rates between 0 and $\sigma_{1,2}I$ followed by integration over the Gaussian profile of the focused beam. Indeed, as the blue fluorescence is recolted from an extremely thin part of the sample, we may assume that the dimming of the pump beam across the sample does not affect the signal so that the mean value of the measured fluorescence is given by $\langle f\rangle = \int_0^\infty f(r) 2\pi r\, dr$ in which $f(r)$ is the recolted fluorescence coming from a ring of radius r of the input beam. Then, as for a beam waist r_0, $I=(I_0/\pi r_0^2)e^{(-r^2/r_0^2)}$, $\langle f\rangle$ is given by

$$\langle f\rangle = \pi r_0^2 \int_0^{I_0} \frac{f(I)}{I}\, dI.$$

All the experimental curves are nicely fitted with the following parameters:

TABLE I. Spectroscopic parameters of the YAG:5 at. % Tm^{3+} at 35 K. The b_{ij} values are calculated using the Ω_t intensity parameters given in Ref. 38.

τ_2 (ms)	12 (Ref. 36)
W_3 (ms^{-1})	0.585 (Ref. 33)
W_3^{NR} (ms^{-1})	0.900 (Ref. 33)
W_4 (ms^{-1})	1.75 (Ref. 33)
b_{ij}	$b_{32}=0.18$ $b_{42}=0.43$ $b_{43}=0.14$
s_3 (ms^{-1})	40 (Ref. 34)
s_4 (ms^{-1})	17 (Ref. 33)
Q_{ij} (ms^{-1})	$Q_{22}=0.92$ $Q_{23}=0.26$ (Ref. 28)

$$R_2 = 0.82 \pm 0.25\ \ 10^{-20} I,$$

$$R_1 = 5 \pm 0.5\ \ 10^{-4} R_2. \qquad (26)$$

The theoretical transient curves are presented in Fig. 4 in continuous lines. For comparison, theoretical curves calculated without such integration are also drawn in dotted lines. The impact of the Gaussian shape of the beam on the rise shapes is as predicted phenomenologically before in this section. The apparent experimental threshold is equal to $1.3I_{\text{th}}$ ($I_{\text{th}}=1.9$ kW cm^{-2}). Concerning the evolution of the populations versus pumping power, Fig. 7 shows the nice agreement between theory and experiments provided that the shape of the beam is taken into account. In particular, in the case of the metastable state population, instead of a rapid buildup and subsequent depletion for excitation intensity higher than $10I_{\text{th}}$ predicted by a top hat beam, the Gaussian integration leads to a continuous smooth buildup consistent with experimental results.[9]

Equation (26), gives the excited state absorption cross section σ_2. We find $0.82\pm0.25\ 10^{-20}$ cm^2 at 35 K. At room temperature, photon avalanche is always efficient in this material[14] and, using the same fitting procedure we find $\sigma_2=0.32\pm0.1\ 10^{-20}$ cm^2. By recording excited state excitation spectrum of the $^1G_4 \rightarrow {}^3H_6$ fluorescence at room temperature, the measured value of σ_2 was 0.4×10^{-20} cm^2.[35] This is in close agreement with our result and confirms the validity of our model.

V. CONCLUSION

We have shown that the rate equation analysis describes well the photon avalanche. We developed for this two arguments. The first one is theoretical: as the avalanche is a bifurcation, we may use the mean-field approach to describe it without losing any physical meaning. The second one is experimental: the fits work very well, with only two fitting parameters, providing that the input intensity profile of the beam is taken into account.

The photon avalanche effect arises from the microscopic

interactions between ions (cross relaxation) which connect them each other. The excited state pumping rate controls these interactions by allowing them or not. This microscopic process leads to a bifurcation phenomenon when the interactions are strong enough to put all the ions in the same state. The Landau theory approach gives a very clear description: the microscopic interactions between ions, with the excited state pumping rate, induce a macroscopic force which leads to avalanche by connecting the ions to each other. The potential, deduced from the force, is controlled by the excited state pumping rate. This control parameter induces a fundamental change of the potential curve which leads to a very simple bifurcation diagram. The transient signal of the fluorescence is directly linked to the shape of the potential. So, the experimental signature of the avalanche is a change of the dynamics with an important slowing down at the threshold point.

We have given the analytical expression of the upconverted fluorescence at the threshold and, thus, of the critical slowing down. This critical slowing down is directly linked to the ratio β of the nonresonant ground state over the resonant excited state absorption cross sections. We have shown that the more β is weak the more this experimental signature of the photon avalanche will be spectacular. We have discussed the limit value of β for which the photon avalanche remains the main pumping channel for the upconverted fluorescence. That limit depends clearly on the spectroscopic characteristics of the rare earth ion which are connected to the host matrix and to the rare-earth concentration in this host.

The reconciliation between rate equations and experimental results allowed us to investigate systematically the impact of the different parameters entering the model[36] and to discuss the efficiency of such an avalanche process in several thulium doped bulk or waveguide materials.[36] These two aspects will be the subjects of future papers.

ACKNOWLEDGMENTS

We acknowledge Professor J. L. Barrat from the DPM Université Lyon 1 and Dr. L. Bocquet from the Laboratoire de Physique ENS Lyon for helpful discussions. We thank Z. Frukacz from ITME Laboratory (Warsaw, Poland) for providing us with the single crystals used in this study.

APPENDIX: EXPRESSION OF THE CONSTANTS IN THE SIMPLEST CASE

In the simplest photon avalanche case, only three levels are involved[2] and the rate equation system is simplified in

$$dn_3/dt = R_2 n_2 - W_3 n_3 - s_3 n_3 n_1,$$

$$dn_2/dt = R_1 n_1 - (R_2 + W_2) n_2 + b_{32} W_3 n_3 + 2 s_3 n_1 n_3 - Q_{22} n_2^2,$$

$$n_1 + n_2 + n_3 = 1.$$

This is the same system as in Ref. 2 except that we add the $Q_{22} n_2^2$ term which takes into account the saturation effect from the metastable state.[37] As the level 2 as a much longer lifetime than the level 3 we may use the adiabatic approximation. This leads to the same expressions for the Eqs. (9) to (25) with the following constants:

$$a = b = 1,$$

$$c = (2 - \tau_3 W_{32}) \tau_3 s_3,$$

$$Q = Q_{22},$$

$$R_{2\text{th}} = W_2 / (\tau_3 W_{32} - 1).$$

As a matter of fact, whatever is the avalanche system, there is always a metastable level and so, the same calculation could be done leading to the same potential.

[1] J. S. Chivian, W. E. Case, and D. D. Eden, Appl. Phys. Lett. **35**, 124 (1979).

[2] W. Lenth and R. M. Macfarlane, J. Lumin. **45**, 346 (1990).

[3] R. M. Macfarlane, R. Wannemacher, T. Hebert, and W. Lenth, *Conference on Lasers and Electro-Optics*, 1990 *Technical Digest Series* (Optical Society of America, Washington, DC, 1990), Vol. 7, p. 250; T. Hebert, R. Wannemacher, R. M. Macfarlane, and W. Lenth, Appl. Phys. Lett. **60**, 2592 (1992).

[4] D. C. Hanna, R. M. Percival, I. R. Perry, R. G. Smart, J. E. Townsend, and A. C. Tropper, Opt. Commun. **78**, 187 (1990).

[5] U. Oetliker, M. J. Riley, P. S. May, and H. U. Güdel, J. Lumin. **53**, 553 (1992); Coord. Chem. Rev. **111**, 125 (1991).

[6] N. Pelletier-Allard and R. Pelletier, Opt. Commun. **81**, 247 (1991).

[7] H. Ni and S. C. Rand, Opt. Lett. **16**, 1424 (1991).

[8] M. F. Joubert, S. Guy, and B. Jacquier, Phys. Rev. B **48**, 10 031 (1993); M. F. Joubert, S. Guy, B. Jacquier, and C. Linarès, Opt. Mater. **4**, 43 (1994).

[9] A. W. Kueny, W. E. Case, and M. E. Koch, J. Opt. Soc. Am. B **10**, 1834 (1993).

[10] B. C. Collings and A. J. Silversmith, J. Lumin **62**, 271 (1994).

[11] F. Auzel, Y. Chen, and D. Meichenin, J. Lumin. **60** & **61**, 692 (1994).

[12] Y. Chen and F. Auzel, Electron. Lett. **30**, 1602 (1994); J. Non Cryst. Solids **184**, 57 (1995); J. Phys. Condens. Matter **7**, 3363 (1995).

[13] R. Sheps, IEEE J. Quantum Electron. **30**, 2914 (1994); **31**, 309 (1995).

[14] S. Guy, M. F. Joubert, and B. Jacquier, Phys. Status Solidi B **183**, K33 (1994).

[15] S. Guy, M. F. Joubert, B. Jacquier, and C. Linares, Radiat. Eff. Def. Solids **133–134**, 65 (1995).

[16] C. Borel, A. Rameix, Ph. Thony, B. Ferrand, D. P. Shepherd, A. C. Large, T. J. Warburton, A. C. Tropper, D. C. Hanna, S. Guy, M. F. Joubert, and B. Jacquier, in *OSA Proceedings on Advanced Solid State Lasers*, edited by B. H. T. Chai and S. A. Payne (Optical Society of America, Washington, DC, 1995), Vol. 24, p. 37.

[17] M. Bouffard, J. P. Jouart, and G. Mary, Phys. Status Solidi B **193**, 239 (1996).

[18] M. F. Joubert, S. Guy, C. Linarès, B. Jacquier, and J. L. Adam, J. Non Cryst. Solids **184**, 98 (1995).

[19] S. Guy, D. P. Shepherd, M. F. Joubert, B. Jacquier, and H. Poignant, J. Opt. Soc. Am. B (to be published).

[20] E. Bielejec, E. Kisel, and A. J. Silversmith (unpublished).
[21] F. Auzel and Y. Chen, J. Lumin. **65**, 45 (1995).
[22] T. Sandrock, E. Heumann, G. Huber, and B. H. T. Chai, in *OSA Proceedings on Advanced Solid State Lasers*, edited by Stephen A. Payne and Clifford Pollock (Optical Society of America, Washington, DC, 1996), Vol. 1, p. 550.
[23] M. Bouffard, J. P. Jouart, and G. Mary, J. Phys. **6**, 691 (1996).
[24] W. E. Case, M. E. Koch, and A. W. Kueny, J. Lumin. **45**, 351 (1990).
[25] M. F. Joubert, S. Guy, B. Jacquier, and C. Linares, J. Appl. Spectrosc. **62**, 126 (1995).
[26] C. Normand, Y. Pomeau, and M. G. Velarde, Rev. Mod. Phys. **49**, 581 (1977).
[27] S. R. Bowman, J. G. Lynn, S. K. Searls, B. J. Feldman, J. McMahon, W. Whitney, C. Marquardt, D. Epp, G. J. Quarles, and K. J. Ryley, in *Advanced Solid-State Lasers*, OSA Proceedings Series, Vol. 15, edited by A. A. Pinto and T. Y. Fan (Optical Society of America, Washington, D. C., 1993), p. 415.
[28] L. B. Shaw, R. S. F. Chang, and N. Djeu, Phys. Rev. B **50**, 6609 (1994).
[29] L. D. Landau and I. M. Lifshitz, *Course of Theoretical Physics* (Pergamon, London-Paris, 1959), Vol. 5.
[30] A. Brenier, L. C. Courrol, C. Pedrini, C. Madej, and G. Boulon, Opt. Mater. **3**, 25 (1994).
[31] Ph. Goldner and F. Pellé, Opt. Mater. **5**, 239 (1996).
[32] A. W. Kueny, W. E. Case, and M. E. Koch, J. Opt. Soc. Am. B **6**, 639 (1989).
[33] S. Guy, M. Malinowski, Z. Frukacz, M. F. Joubert, and B. Jacquier, J. Lumin **68**, 115 (1996).
[34] G. Armagan, A. M. Buoncristiani, and B. Di Bartolo, Opt. Mater. **1**, 11 (1992).
[35] N. Garnier, R. Moncorgé, H. Manaa, E. Decroix, P. Laporte, and Y. Guyot, J. Appl. Phys. **79**, 4323 (1996).
[36] S. Guy, Thèse de Doctorat, Université C. Bernard, 1995.
[37] Y. Guyot, H. Manaa, J. Y. Rivoire, R. Moncorgé, N. Garnier, E. Descroix, M. Bon, and P. Laporte, Phys. Rev. B **51**, 784 (1995).
[38] W. F. Krupke (unpublished).